Journal of Energy Chemistry 26 (2017) 398–405

Contents lists available at ScienceDirect

Journal of Energy Chemistry

journal homepage: www.elsevier.com/locate/jechem

http://www.journals.elsevier.com/journal-of-energy-chemistry/

A simple and distinguished nebulizer approach to prepare CdS thin films

M. Girish[a], R. Sivakumar[a,*], C. Sanjeeviraja[b], R. Gopalakrishnan[c]

[a] Department of Physics, Alagappa University, Karaikudi 630003, India
[b] Department of Physics, Alagappa Chettiar College of Engineering and Technology, Karaikudi 630003, India
[c] Department of Physics, Anna University, Chennai 600025, India

ARTICLE INFO

Article history:
Received 13 October 2016
Revised 24 November 2016
Accepted 5 December 2016
Available online 21 December 2016

Keywords:
Semiconductors
Chemical synthesis
Optical properties
X-ray diffraction

ABSTRACT

In this paper, we report the substrate temperature induced change in structural, optical, morphological, luminescence and photoelectrochemical properties of CdS films deposited by a simple and facile approach called nebulized spray pyrolysis technique. X-ray diffraction study confirmed the deposited CdS films belong to hexagonal wurtzite structure, with preferential orientation along *c*-axis, (002) direction perpendicular to the substrate plane. The crack free, uniform, and homogeneously distributed spherical particles are witnessed from AFM image. Various optical parameters like energy band gap, optical conductivity, refractive index, extinction coefficient, dielectric constants, and dispersion energy parameters of the films were evaluated. The strong band edge emission observed in the PL study may be attributed to the recombination of excitations and/or shallowly trapped electron-hole pairs. The first and second overtone of LO modes of CdS at 302 and 600 cm^{-1} are observed in the Raman study. The photoelectrochemical properties of the films were also tested.

1. Introduction

Cadmium sulfide (CdS) is a most important member of metal chalcogenide family (II–VI group) having *n*-type semiconducting nature and it has been considered as one of the most promising window layer materials for heterojunction thin film solar cells [1,2], photovoltaic devices [3,4], and photo sensors [5] because of its intermediate band gap (2.42 eV), high absorption coefficient, electron affinity and low resistivity. For solar cell applications, CdS films need to have a suitable conductivity ($>10^6$ carriers/cm^3) with adequate thickness to allow high transmission. Thin film based photoelectrochemical (PEC) solar cells have wide applications due to their low fabrication cost, high throughput processing techniques and ease of junction formation with an electrolyte. The semiconductors with band gap close to the maximum wavelength in the visible spectrum are promising materials for the PEC cells. Hence, CdS is one of the promising semiconductors for PEC studies.

Although high-quality polycrystalline CdS films can be produced using vapor epitaxial growth techniques [6,7] or sputtering [8,9], the fabrication cost increases significantly. Since CdS compound is an expensive material, several studies were developed towards the polycrystalline compound semiconductors, especially polycrystalline thin films. Spray pyrolysis is a widely used method for producing polycrystalline CdS films [10]. This is a convenient, fast and relatively low-cost process which has been used for the deposition of thin films for many years. Spray pyrolysis technique is a simple technology which involves many processes such as aerosol generation and transport, solvent evaporation, droplet impact with consecutive spreading and precursor decomposition. The substrate temperature is implicated in all above mentioned processes, except in the aerosol generation. Therefore substrate temperature has a vital role in determining the morphology and other physical properties of the deposited films.

In present work, we have employed the nebulized spray pyrolysis technique (NSP) for the fabrication of polycrystalline CdS thin films which has not yet been reported to the best of our knowledge. Unlike sophisticated apparatus, NSP consists of only hot furnace, temperature controller, compressor and nebulizer with a spray nozzle. In NSP technique, carrier gas is pumped directly in to the solution thereby enhancing the atomization of particles inside the nebulizer. The atomized particles are brought to the substrate through the '*L*' shaped glass tube which acts as the spray nozzle. In conventional spray technique, though the solution is pulverized by means of air and the atomized particles reach the substrate, thereby the deposition of large droplets take place. Thus, the generated aerosol does not get proper atomization. NSP technique avoids these shortcomings to fabricate homogeneous CdS

* Corresponding author.
E-mail address: krsivakumar1979@yahoo.com (R. Sivakumar).

http://dx.doi.org/10.1016/j.jechem.2016.12.004

thin films. The basic principle behind the working of the nebulizer is Venturi effect. The Venturi effect is explained as the high velocity movement of fluid, when passed through a constricted tube or pipe causing reduction in the fluid pressure and self-pumping effect. It is a jet effect as with a funnel velocity of the fluid decreases as the cross sectional area decreases as with the static pressure correspondingly decreasing. The spray quality generated by the nebulizers play an important role in various properties of thin films. Within the spray system, the droplet size is one of the most critical factors related to drift. Drift is caused when large droplets retain momentum for a long time and less prone to displacement. The droplet size distribution near the aperture depend on the nozzle size, spray pressure, liquid properties etc. When a fluid flows through a tube that narrows to a smaller diameter, the partial restriction causes a higher pressure at the inlet than that at the narrow end. In addition, the advantage of NSP over conventional pneumatic spray method is that its low material consumption with superior control of the spray particles and very low carrier gas pressure, which leads to get very thin layer of pinhole free films with desired properties.

In this paper, we have studied the structural, optical, morphological and photoelectrochemical properties of CdS thin films deposited by nebulized spray pyrolysis technique. We report, for the first time, the dielectric and dispersion parameters of CdS thin films derived from the optical study.

2. Experimental

CdS thin films were deposited on glass substrates by nebulized spray pyrolysis (NSP) technique. The precursor solution was prepared by dissolving equal amounts of aqueous solutions of 10 mL of 0.16 M cadmium chloride ($CdCl_2$) and 0.16 M thiourea ($CS(NH_2)_2$) and continuously stirred for 15 min to get homogenous solution. The solution thus obtained was sprayed intermittently on well cleaned pre-heated glass substrates by means of nebulized spray pyrolysis at three different substrate temperatures like 300, 350, 400 °C. The intermittent spray interval (30 s) promotes the substrates to attain the expected temperature before the start of next spray. The solution flow was controlled by the pressurized air with a constant pressure of 0.7 kg/cm^2. In this technique, comparatively lesser air pressure is employed, even without any compromise in the quality of thin films. The low flow rate controls the droplet size hence minimizing drift. The distance between nozzle and substrate was 4 cm. The films were deposited for about 30 min. When the substrate temperature is too low (below 300 °C), there is a possibility for the formation of oxide phase during film growth due to the slow dissociation of complexes. On the other hand, at higher substrate temperature (above 400 °C) the re-evaporation of sulphur can take place due to its elevated vapor pressure. Therefore, the substrate temperature was optimized between 300 and 400 °C. The deposited films were observed as yellow in color, well adherent to the substrate, pin hole free, and uniform in nature. The thickness of deposited film varies between 0.68 and 0.71 μm as observed from the surface profilometer (Mitutoyo, SJ-301).

The structural property of CdS thin films were studied by X-ray diffraction (XRD) using CuK_α ($\lambda = 0.154$ nm) radiation source (X'Pert Pro PANalytical) over 2θ scan range of 10–70°. The effect of substrate temperature on the change in optical property of CdS film was studied using UV–Vis–NIR spectrophotometer (Ocean optics HR2000). The room temperature photoluminescence (PL) study was performed using a fluorescence spectrophotometer (Varian Cary Eclipse). Vibrational property of the film was studied using micro Raman spectrometer system (LABRAM HR-800) using 488 nm line of Ar^+ -ion laser with a power of 10 mW. Surface morphological study was carried out using atomic force microscope (AFM; Nanoscope-E). The compositional nature of the film was tested by energy dispersive X-ray analysis (EDX; INCA OXFORD). The photoelectrochemical (PEC) properties of the film was studied by forming two electrode system consisting of CdS thin film deposited on fluorine doped tin oxide (FTO) coated glass substrate as a working electrode and graphite as a counter electrode with the 0.25 M polysulphide electrolyte solution. Current–voltage (I–V) characteristics of the PEC cells were measured by solar simulator (4200 Keithley semiconductor characterization system) under illumination using a halogen lamp with an intensity of 10 mW/cm^2.

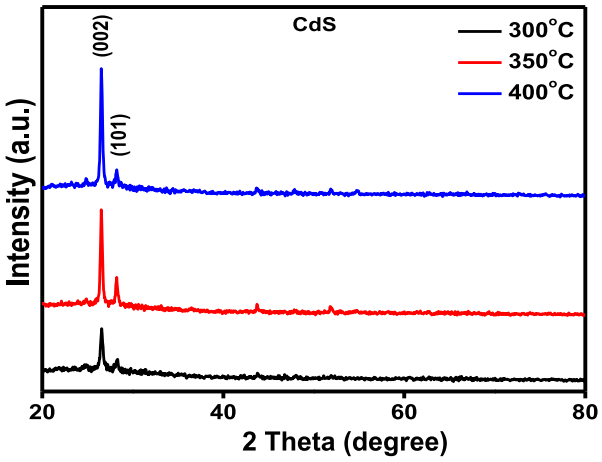

Fig. 1. XRD patterns of CdS thin films.

3. Results and discussion

3.1. X-ray diffraction

Fig. 1 shows the X-ray diffraction patterns of CdS thin films deposited at 300, 350, and 400 °C. It is observed that all the films are highly crystalline in nature. The observed lattice spacings (d) were matched very well with JCPDS data (card No.: 77-2306), which confirmed the hexagonal wurtzite structure, with a preferential orientation along the c-axis, (002) direction perpendicular to the substrate plane.

The lattice constants of deposited CdS films are found as $a = 0.596$ nm; $c = 0.400$ nm (hexagonal), which agreed well with JCPDS data. The substrate temperature induced enhancement in degree of (002) peak intensity revealed the increase in crystalline nature of deposited films. At higher substrate temperature, atomic, ionic or molecular species of CdS on the substrate surface acquire more thermal energy which leads to the large adatom mobility. This leads to the formation of more number of nucleus which coalesces to form a continuous film with high crystalline nature. Ashour [11] has observed the improved crystallization of CdS films with increase in substrate temperature. From the XRD result we have evaluated various structural parameters viz. crystallite size (D), dislocation density (δ), strain (ε), and lattice distortion (LD) using the following relations [12–14] $D = 0.94\ \lambda/\beta\ \cos\theta$, $\delta = 1/D^2$, $\varepsilon = \beta\ \cos\theta/4$, $LD = \beta/4\ \tan\theta$, where β is full width at half maximum (FWHM) (in radians) of the XRD peak and the evaluated data are presented in Table 1. One can observe from Table 1 that the average crystallite size of the films increase (37–69 nm) with increasing substrate temperature, which clearly demonstrate the enhancement in degree of crystallinity of films with substrate temperature. On the other hand, the strain, dislocation density and lattice distortion are gradually decreased with increase in substrate temperature. This revealed the decrease in concentration of lattice imperfections since the internal microstrain reduced within the films. It may be mentioned that the dislocation density and the lattice

Table 1. Structural parameters of CdS thin films.

Substrate temperature (°C)	Crystallite size (nm)	Strain ($\times 10^3$ lines^{-2} m^{-4})	Dislocation density ($\times 10^{15}$ lines/m^2)	Lattice distortion (10^{-3})
300	37	0.944	0.730	0.847
350	41	0.654	0.594	0.688
400	69	0.453	0.210	0.640

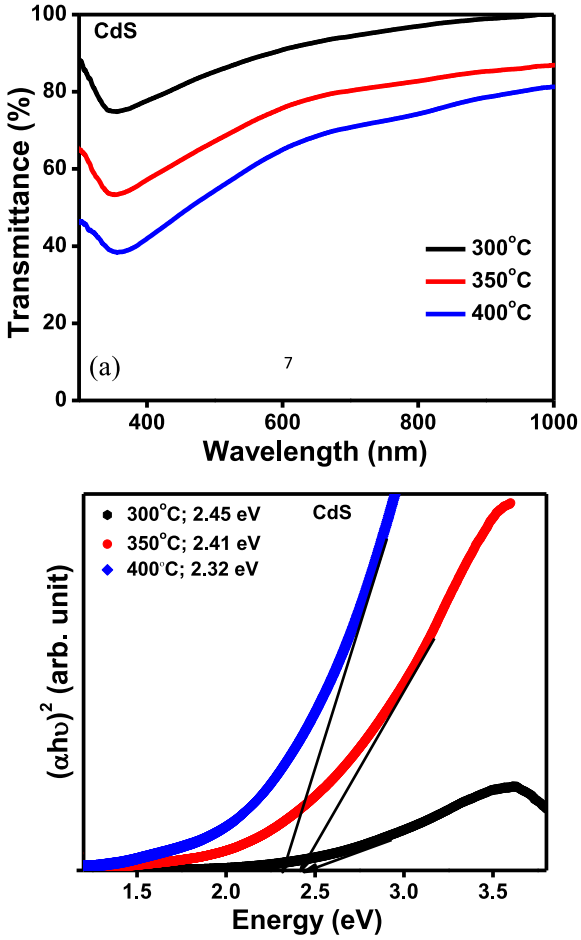

Fig. 2. (a) Transmittance spectra and (b) Tauc plots of CdS thin films.

strain are the manifestation of dislocation network in the films and hence the decrease in dislocation density and strain revealed the formation of good quality films at higher substrate temperature.

3.2. Optical properties

3.2.1. Transmittance, energy band gap, and optical constants

The optical properties of NSP deposited CdS thin films were studied by UV–Vis–NIR spectrophotometer. Fig. 2(a) shows the optical transmittance spectra of CdS thin films deposited at different substrate temperatures. It may be mentioned that the transmittance of CdS film strongly depends on the film structure, which is determined by the preparation methods, film thickness and deposition conditions [10]. It is observed that the transmittance decreases with increase in substrate temperature. This may be attributed to the enhancement in crystallinity and grain growth of films with substrate temperature [15]. Thus, the carrier concentration and surface topography of the film demands the variation in the transmittance of CdS thin films. From the optical data, the direct energy band gap, E_g, of the film was extracted from the traditional Tauc plot of $(\alpha h\upsilon)^2$ versus photon energy E $(=h\upsilon)$ for direct inter-band transitions and is shown in Fig. 2(b) as a function of substrate temperature. A systematic reduction in the band gap with increase in substrate temperature is observed here. The optical band gap values vary from 2.45 to 2.32 eV. A significant variation in crystallite size for the film deposited at 400°C may be the reason for decreased band gap. The observed E_g values are consistent with the reported value of CdS thin films prepared by spray pyrolysis technique [16].

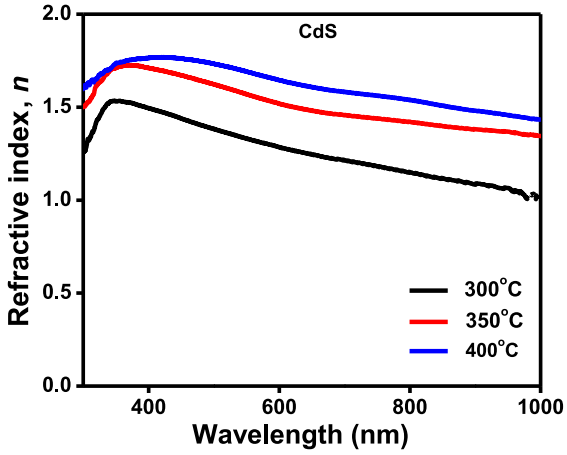

Fig. 3. Refractive index of CdS thin films.

The refractive index plays a vital role in the search for optically active materials, being a significant factor in optical communication and in designing devices for spectral dispersion. If the absorption is high with minimal interference, the refractive index (n) of film can be calculated according to Born and Wolf [17]:

$$R = \frac{n^2+1}{n^2-1} \tag{1}$$

$$n = \frac{1+R+\sqrt{R}}{1-R} \tag{2}$$

where R is the reflectance of the film. The dependence of refractive index (n) as a function of wavelength for CdS thin films at different substrate temperatures is depicted in Fig. 3. The 'n' value is found to be maximum at higher substrate temperatures and decreases with increase in wavelength. Thus, the higher substrate temperature favors the denser films as well as high refractive index [18]. It is also found that the higher value of refractive index at lower wavelength region. This may be due to the quality between the frequency of incident photon and plasma frequency. Anomalous dispersion of refractive index was prevailed in the region of plasma frequency. The refractive index becomes mostly imaginary, when λ crosses λ_p (plasma wavelength) and the corresponding dielectric constant becomes negative [18]. The extinction coefficient (k) can be determined using the following relation [19]:

$$k = \frac{\alpha\lambda}{4\pi} \tag{3}$$

Fig. 4 shows the spectral variation of extinction coefficient as a function of wavelength. The k value increases with increase in substrate temperature. This may be attributed to the transitions

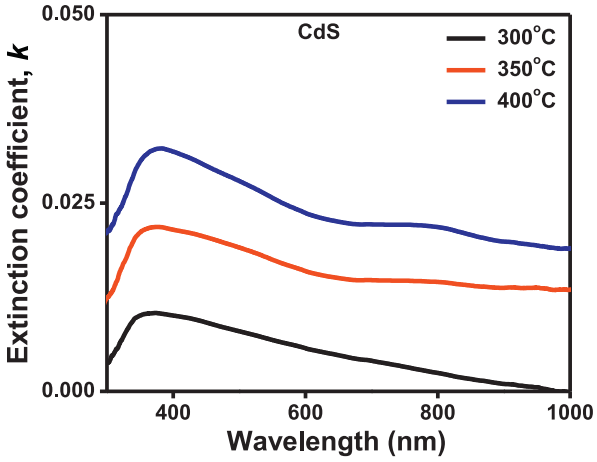

Fig. 4. Extinction coefficient of CdS thin films.

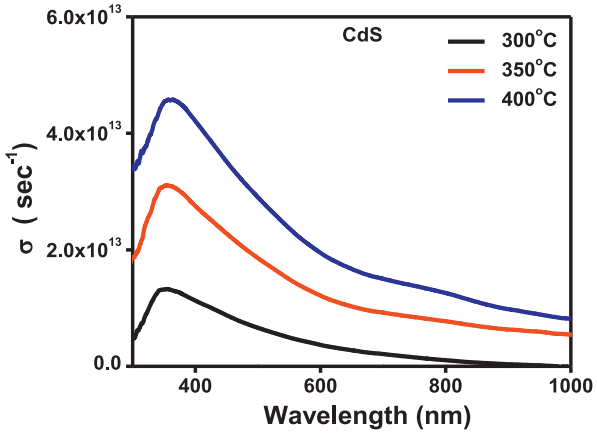

Fig. 5. Optical conductivity of CdS thin films.

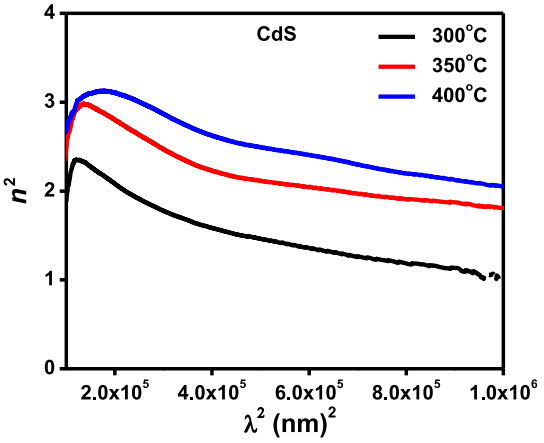

Fig. 6. Plot of n^2 and λ^2 of CdS thin films.

that occur between valence and partly filled conduction band. In addition, this increase in k value with substrate temperature may be due to the increase in surface roughness of the film, which in turn increases the scattering loss thereby decreasing the transmitting ability. This hypothesis is consistent with the optical transmittance data. The variation in optical conductivity (σ_{op}) as a function of photon energy ($h\upsilon$) is shown in Fig. 5 and it can be determined using the following relation [20]:

$$\sigma_{op} = \frac{\alpha nc}{4\pi} \tag{4}$$

where c is the velocity of light. Fig. 5 shows that the optical conductivity drastically increases with increasing substrate temperature. The optical conductivity is found to increase sharply for lower wavelength values due to the large absorption coefficient. This may be due to the low energy band gap values which favor the formation of more excitons by incident photon energy.

3.2.2. Lattice dielectric constant

The relation between refractive index (n), wavelength (λ) and lattice dielectric constant ($\varepsilon_L = n^2$) [21] is given by

$$\varepsilon = n^2 = \varepsilon_{(L)} - \left(\frac{e^2}{4\pi c^2 \varepsilon_0}\right)\left(\frac{N}{m*}\right)\lambda^2 \tag{5}$$

where ε_L is the lattice dielectric constant, e is the electronic charge, c is the velocity of light, ε_0 is free space dielectric constant (8.854×10^{-12} F/m), and N/m^* is the ratio between free carrier density and free carrier effective mass. The variation of n^2 versus $(\lambda)^2$ is shown in the Fig. 6. It can be seen that the values of n^2 is linear at higher wavelength. The values of ε_L and N/m^* of CdS films are presented in Table 2 and these values were determined from the intercepts and slopes of curves shown in Fig. 6. The ε_L value varies from 2.007 to 3.033. The values of N/m^* varies from 2.801×10^{56} cm^{-3}.g^{-1} to 4.168×10^{56}s cm^{-3}.g^{-1}. The increased values of both ε_L and N/m^* with substrate temperature is due to the higher carrier concentration. Plasma frequency (ω_p) is the characteristic frequency at which the electrons couple with the oscillating electric field and is given by the following relation.

$$\omega_p^2 = \frac{e^2 N}{\varepsilon_0 m*} \tag{6}$$

From the above relation, it is clear that the plasma frequency is proportional to N/m^* and the evaluated ω_p values are reported in Table 2. The abundance of charge carriers definitely influences the increment in plasma frequency. These results agree well with the optical conductivity data.

3.2.3. High frequency dielectric constant

Using the dispersion relation of incident photon, the determination of dielectric constant could be defined. The refractive index n can further be analyzed to determine the average interband oscillator wavelength (λ_0) and the average oscillator strength (S_0) of CdS films using the following single Sellmeier oscillator at low energies [22].

$$\frac{\left(n_0^2 - 1\right)}{\left(n^2 - 1\right)} = 1 - \left(\frac{\lambda_0}{\lambda}\right)^2 \tag{7}$$

where $n_{0(1)}$ is the static refractive index, which provides a good indication on the structure and density of the material. According to Moss model [23] the contribution of free carriers to the dispersion are very small. This means that the data corresponding to the wavelength range lying below the absorption edge of the material has to be used to evaluate ε_∞ [24].

$$n^2 - 1 = \frac{S_0 \lambda_0^2}{1 - \left(\frac{\lambda_0}{\lambda}\right)^2} \tag{8}$$

and the S_0 is defined as

$$S_0 = \frac{\left(n_\infty^2 - 1\right)}{\lambda_0^2} \tag{9}$$

Fig. 7 shows the plot of $(n^2-1)^{-1}$ and λ^{-2} as a function of different substrate temperature. In this graph the intersection with $(n^2-1)^{-1}$ axis which is $(n_0{}^2-1)^{-1}$ and hence, n_∞^2 at λ_0 is equal

Table 2. Optical dielectric parameters of CdS films.

Substrate temperature (°C)	ε_L	ε_∞	n_0 $n_{0(1)}$	$n_{0(2)}$	λ_0	$S_0 \times 10^{12}$	$N/m^* \times 10^{56}$ (cm^{-3}•g^{-1})	ω_p (Hz) $\times 10^{14}$	τ (s) $\times 10^{-15}$
300	2.007	1.262	1.416	1.123	482	1.128	2.801	9.001	1.110
350	2.572	1.577	1.603	1.255	530	2.051	3.291	9.756	1.025
400	3.033	1.704	1.741	1.305	625	1.800	4.168	10.980	0.910

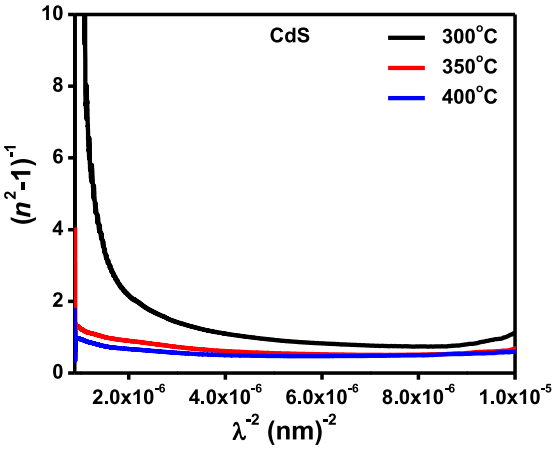

Fig. 7. Plot of $(n^2-1)^{-1}$ and λ^{-2} of CdS thin films.

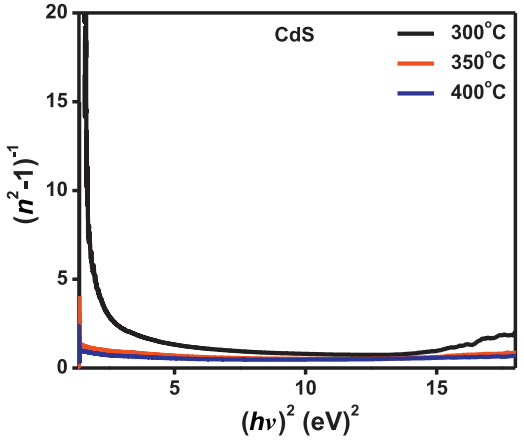

Fig. 8. Plot of $(n^2-1)^{-1}$ and $(h\upsilon)^2$ of CdS thin films.

to high frequency dielectric constant (ε_∞). The evaluated values of $n_{0(1)}$, ε_∞, λ_0 and S_0 are reported in Table 2. These values are of the same order of magnitude as those obtained by Wemple and DiDomenico for material like ZnO [25].

3.2.4. Dispersion parameters and dielectric relaxation time

Using the single-oscillator approximation, Wemple and DiDomenico [25] have developed a model where the refractive index dispersion is studied in the region of transparency below the gap. Defining two parameters, the oscillation energy E_0, and the dispersion energy E_d, this model concludes that:

$$n^2(h\nu) = 1 + \frac{E_0 E_d}{E_0^2 - (h\nu)^2} \tag{10}$$

Fig. 8 shows the plot of $(n^2-1)^{-1}$ and $(h\upsilon)^2$ of CdS thin films deposited at different substrate temperatures. The energy oscillation and dispersion energy values were evaluated from the slope and intercept of the curves, respectively and the values are given in Table 3. The dispersion energy measures the average strength of interband optical transitions. The E_0 and E_d values increase due to

Table 3. Dispersion parameters of CdS films.

Substrate temperature (°C)	E_0 (eV)	E_d (eV)	E_l (eV)	E_g (eV)
300	2.141	0.308	1.189	2.45
350	3.116	2.361	1.426	2.41
400	3.140	3.206	2.062	2.32

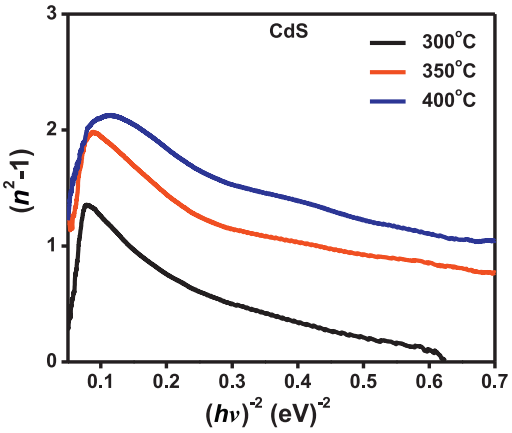

Fig. 9. Plot of (n^2-1) and $(h\upsilon)^{-2}$ of CdS thin films.

the increase in thickness [26]. Wemple and DiDomenico have related this parameter to the coordination number of the anion and the number of valence electrons per anion. The optical parameters such as E_0 and $E_{d,}$ can be correlated with the lattice energy, which gives information about the strength of the bonds in an ionic compound. It describes the binding force between the atoms. E_l can be evaluated using the following relation [27]:

$$n^2 - 1 = \frac{E_d E_0}{E_0^2 - E^2} - \frac{E_l^2}{E^2} \tag{11}$$

where E_l is the lattice energy. Plotting graph between (n^2-1) and $(h\nu)^{-2}$ (Fig. 9) and taking slope gives E_l^2. The calculated E_l values are reported in the Table 3 and its magnitude is increasing with substrate temperature. This may be probably due to the strengthening of Cd–S bonds at higher substrate temperatures. The static refractive index $n_{0(2)}$ (the zero-frequency refractive index) of CdS films can be calculated by extrapolating the Wemple and DiDomenico dispersion relation to the value of the incident photon energy approaching zero [10] as given by the following equation.

$$n_0^2 = 1 + \frac{E_d}{E_0} \tag{12}$$

It is observed from Table 2 that the calculated $n_{0(2)}$ values are comparable with the values of $n_{0(1)}$ as evaluated in the earlier Section 3.2.3.

The dielectric relaxation time (τ) can be calculated using the relation $\omega_p \times \tau = 1$. As seen from the Table 2 that the τ value decrease with increasing substrate temperature, which may be due to the higher carrier concentration of CdS thin films upon increasing the substrate temperature. This inference may be related with the plasma frequency and optical conductivity data where the carrier concentration determines the steadiness in conductivity.

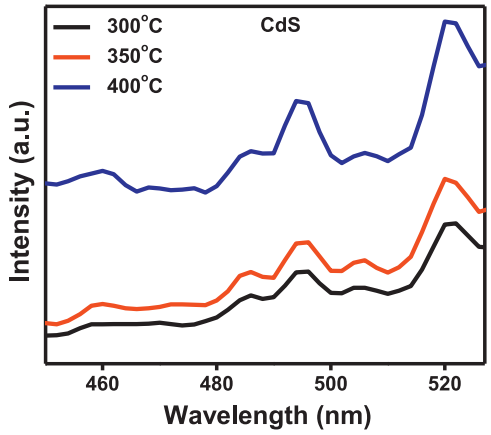

Fig. 10. Photoluminescence spectra of CdS thin films.

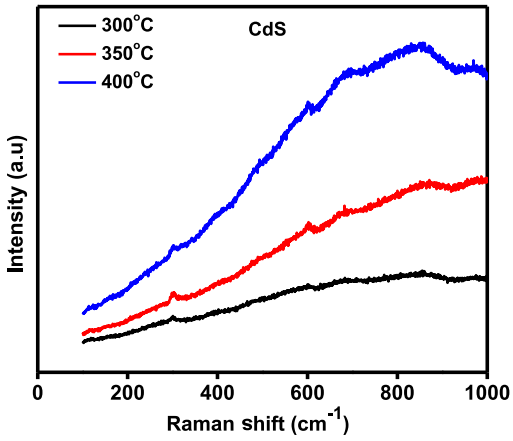

Fig. 11. Raman spectra of CdS thin films.

3.3. Photoluminescence study

Photoluminescence (PL) spectroscopy can be used to determine the band gap of semiconductors since the most common radiative transition in the semiconductor occurs between states at the bottom of the conduction band and the top of the valence band [10]. Fig. 10 represents the room-temperature PL spectra of CdS thin films deposited at different substrate temperature. The films were excited at the wavelength of 280 nm. PL bands appearing in the energy range of 2.18–2.54 eV are called green bands; bands appearing between 2.07 and 2.18 eV are typically referred to as yellow bands; the orange band is located between 2 and 2.07 eV, and the luminescence observed around 1.54–2 eV is called the infrared / red band [16].

Luminescence in the green band (2.51 eV) is observed for all the samples. The appearance of strong band edge emission may be attributed to the recombination of excitations and/or shallowly trapped electron-hole pairs. As calculated from the optical absorption study, the E_g of CdS films vary between 2.45 and 2.32 eV and the band edge emission peak observed in the PL study is about 2.4 eV, which shows the consistency of our optical results.

3.4. Raman spectroscopy

Fig. 11 illustrates the Raman spectra of CdS thin films deposited at 300, 350, and 400 °C. It may be mentioned that the intensities of the fundamental and first overtone of the longitudinal optic (LO) phonons can be used for qualitative understanding of electron–phonon interaction in small particles. Raman peaks observed at about 302 cm^{-1} are corresponding to 1LO and the peak observed at about 600 cm^{-1} is corresponds to 2LO. The position of 1LO peak of bulk sample was reported as 305 cm^{-1} [28]. The reduced LO phonon energy is characterized by lattice softening of CdS thin films [29]. The broad background for CdS thin film deposited at 400 °C is attributed to photoluminescence superimposed signal [30].

Table 4. PEC cell parameters of CdS thin films.

Substrate temperature (°C)	I_{sc} (mA/cm^2)	V_{oc} (V)	Fill factor FF (%)	Efficiency η (%)
300	0.246	0.077	34.6	0.06
350	0.405	0.080	38.5	0.12
400	0.707	0.093	39.2	0.25

3.5. AFM and EDX studies

Atomic force microscopy (AFM) is one of the most effective ways for surface analysis due to its high resolution. The morphology and surface features of thin films could be controlled by varying the deposition parameters such as precursor concentration, carrier gas pressure, substrate temperature, and reducing the droplet size in order to get a homogenous film. Fig. 12 shows the AFM image and histogram of CdS thin film deposited at 400 °C. The complete formation of homogenous spherical crystal grains are observed in the AFM image, which revealed the high crystalline nature of the film deposited at 400 °C.

This is independently corroborated by our X-ray diffraction measurement. From the histogram the root mean square surface roughness of the film is evaluated as 12.6 nm. The compositional nature of CdS thin film deposited at 400 °C was analyzed by EDX. In this study, no other impurity was observed other than the Cd and S elements (spectrum not shown here), which revealed the compositional purity of deposited film. In addition, the S/Cd ratio is measured as 0.9, which indicates the stoichiometric nature of the prepared film.

3.6. Photoelectrochemical study

When a photoelectrode is immersed in an electrolyte an electrode–electrolyte interface is formed which is called PEC cell. Relatively stable and efficient photoelectrochemical solar cells fabricated from transition metal chalcogenide materials exhibit a significant improvement in the electrochemical conversion efficiency. The generation of short circuit current (I_{sc}) and open circuit voltage (V_{oc}) in PEC cell is directly related to the properties of a semiconductor and an electrolyte. As soon as the photoelectrode is immersed in an electrolyte, charge transfer takes place across the interface, which in turn forms depletion region across the interface. This depletion region is driving force for the current–voltage characteristics in dark and under illumination [31]. Fig. 13 shows the *I–V* curves of the PEC cell formed by CdS thin film (deposited on FTO substrate) as a working electrode (active surface area 1 cm^2) and graphite as counter electrode, under the illumination of light using halogen lamp in 0.5 M sulfide/polysulfide redox electrolyte.

From the figure, it is seen that all samples are of *n*-type as the photovoltage behavior is cathodic. The values of I_{sc}, V_{oc}, efficiency (η) and fill factor (FF) are reported in Table 4. The maximum conversion efficiency of 0.25% was obtained for the film deposited at 400 °C. This may be due to thickness, high crystallinity and lower values of strain, dislocation density and lattice distortion. The grain growth induced by the substrate temperature reduces the grain boundaries which in turn reduces the recombination centers for minority charge carriers and trapping centers for majority charge

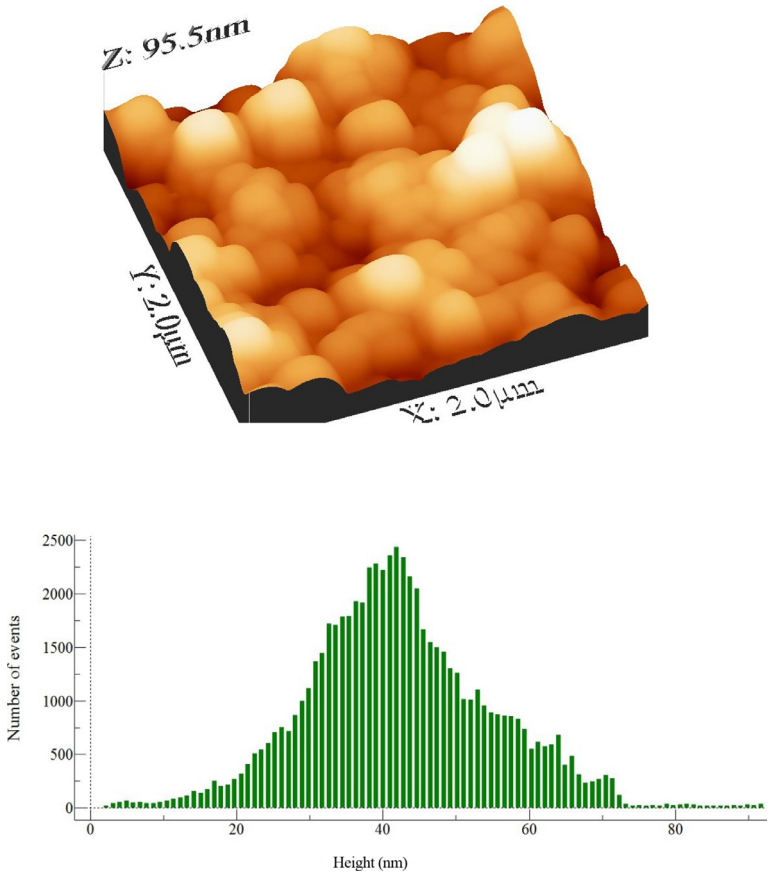

Fig. 12. AFM image and histogram of CdS thin films.

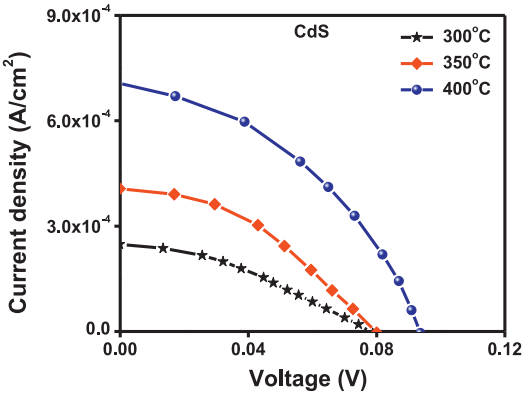

Fig. 13. *I–V* characteristics of CdS thin films.

carriers. This leads to the increase in I_{sc} and V_{oc} with substrate temperature.

4. Conclusions

CdS thin films were prepared by means of distinguished nebulized spray technique. X-ray diffraction study revealed the formation of polycrystalline films with hexagonal wurtzite phase. A systematic reduction in the band gap (2.45 to 2.32 eV) with increase in substrate temperature was observed. The normal dispersion of the refractive index was successfully fitted with the Sellmeier and Wemple formulae. The dispersion energy parameters were determined using Wemple and DiDomenico approximation. The appearance of strong band edge emission in the PL study may be attributed to the recombination of excitations and/or shallowly trapped electron-hole pairs. The high crystalline nature of the film deposited at 400 °C was also evident from the complete formation of homogenous spherical crystal grains in the AFM image. The first and second overtone of LO modes at 302 and 600 cm^{-1} were observed in the Raman study. The substrate temperature induced increase in I_{sc} and V_{oc} of CdS film was realized from the PEC study. From these studies and results, the authors believe that the nebulized spray pyrolysis with inhaler can be used as a potential technique to grow device quality CdS thin films for photoelectrochemical application.

Acknowledgments

One of the authors M. Girish gratefully acknowledges the University Grants Commission (UGC), New Delhi, India for the financial support under UGC-BSR Research Fellowship Scheme. The authors would like to thank the UGC-DAE Consortium for Scientific Research, Indore Centre, India for providing the AFM and Raman facilities. In addition, R.S gratefully acknowledges the UGC, New Delhi, India for the financial support under Major Research Project (Ref.: F.No.42-818/2013(SR), dt.22.03.2013).

References

[1] B. Su, K.L. Choy, Thin Solid Films 359 (2000) 160–164.
[2] C. Thanachayanont, K. Inpor, S. Sahasithiwat, V. Meeyoo, J. Korean Phys. Soc. 52 (2008) 1540–1544.
[3] C.S. Ferekides, D. Marinskiy, V. Viswanathan, B. Tetaly, V. Palekis, P. Selvaraj, D.L. Morel, Thin Solid Films 361 (2000) 520–526.
[4] J. Britt, C. Ferekides, Appl. Phys. Lett. 62 (1993) 2851–2852.
[5] B.K. Maremadi, K. Colbow, Y. Harima, Rev. Sci. Instrum. 68 (1997) 3898–3903.
[6] T.K. Koo, J.H. Park, C.S Kim, Y.M. Yu, D.J. Kim, M.Y. Yoon, Y.D. Choi, J. Korean Phys. Soc. 53 (2008) 202–206.

[7] K.S. Youn, K.H. Yu, J.S. Song, I.H. Choi, J. Korean Phys. Soc. 47 (2005) 89–93.
[8] D.B. Fraser, H. Melchior, J. Appl. Phys. 43 (1972) 3120–3127.
[9] S.G. Hur, E.T. Kim, J.H. Lee, G.H. Kim, S.G. Yoon, Electrochem. Solid-State Lett. 11 (2008) H176–H178.
[10] C. Santiago Tepantlán, A.M. PéRez González, I. Valeriano Arreola, Rev. Mex. F´ıs. 54 (2008) 112–117.
[11] A. Ashour, Turk. J. Phys. 27 (2003) 551–558.
[12] Y. Ji-Beom, L.F. Alan, R.H. Bube, J. Appl. Phys. 68 (1990) 4694–4699.
[13] G.B. Williamson, R.C. Smallman, Phil. Mag. 1 (1956) 34–46.
[14] B. Lonnberg, T. Lundstrom, J. Mater. Sci. 29 (1994) 2993–2997.
[15] N. Abbas, Int. J. Nanoelectron. Mater. 6 (2013) 17.
[16] T. Sivaraman, V.S. Nagarethinam, A.R. Balu, Res. J. Mater. Sci. 2 (2014) 6–15.
[17] M. Born, E. Wolf, Principles of Optics, seventh ed., Cambridge University Press, 2005.
[18] S.A. Mahmoud, S. Alshomer, M.A Tarawnh, J. Modern Phys. 2 (2011) 1178–1186.
[19] Y. Ji-Beom, L.F. Alan, R.H. Bube, J. Appl. Phys. 68 (1990) 4694–4699.
[20] P. Sharma, V. Sharma, S.C. Katyal, Chalcogenide Lett. 3 (2006) 73–79.
[21] T.S. Moss, G.J. Burrell, E. Ellis, Semiconductor Opto-Electronics, Butterworths, London, 1973.
[22] E.R. Shaaban, M. El-Hagary, M. Emam-Ismail, M.B. El-Den, Philos. Mag. 91 (2011) 1679–1692.
[23] T.S. Moss, Optical Properties of Semiconductors, Butterworths Scientific Publications, London, 1959.
[24] E.M. Assim, J. Alloys Compd. 463 (2008) 55–61.
[25] S.H. Wemple, M. DiDomenico, Phys. Rev. B 3 (1971) 1338–1351.
[26] F. Yakuphanoglu, S. Ilican, M. Caglar, Y. Caglar, J. Optoelectron. Adv. Mater. 9 (2007) 2180–2185.
[27] S.H. Wample, Appl. Opt. 18 (1979) 31–35.
[28] M. Cao, L. Li, B.L. Zhang, J. Huang, K. Tang, H. Cao, Y. Sun, Y. Shen, J. Alloys Compd. 530 (2012) 81–84.
[29] Der-San Chuu, Yu-Ching Chang, Cheng-Ying Hsieh, Thin Solid Films 304 (1997) 28–35.
[30] O. Zelaya-Angel, F.de L. Castillo-Alvarado, J. Avendailo-Lopez, A. Escamilla-Esquivel, G. Contreras-Puente, R. Lozada-Morales, G. Torres-Delgadod, Solid State Commun. 104 (1997) 161–166.
[31] Z. Zang, A. Nakamura, J. Temmyo, Opt. Express 21 (2013) 11448–11456.